JPET Fast Forward. Published on August 11, 2010 as DOI: 10.1124/jpet.110.168831

Cyclooxygenase-2 mediates anandamide metabolism in the mouse brain

Sherrye T. Glaser and Martin Kaczocha

Department of Neurobiology and Behavior (STG)

Department of Biochemistry and Cell Biology (MK)

Stony Brook University, Stony Brook, NY 11794

JPET Fast Forward. Published on August 11, 2010 as DOI: 10.1124/jpet.110.168831
This article has not been copyedited and formatted. The final version may differ from this version.

Cyclooxygenase-2 mediates mouse brain anandamide metabolism

Corresponding Author:

Sherrye T. Glaser

Dept of Neurobiology and Behavior

Stony Brook University

Stony Brook, NY 11794-5230

phone: 631-632-8638

fax: 631-632-6661

sherrye.glaser@stonybrook.edu

Text pages: 32

Tables: 1

Figures: 8

References: 30

Words in Abstract: 249

Words in Introduction: 749

Words in Discussion: 1303

Nonstandard abbreviations: cyclooxygenase-2 (COX-2); cyclooxygenase-2 immunoreactivity (COX-2 IR); long term potentiation (LTP); long term depression (LTD); prostaglandin E2 glycerol ester (PGE2G); 2-arachidonoylglycerol (2-AG); anandamide (AEA); fatty acid amide hydrolase (FAAH); monoglyceride lipase (MGL); ethylenediaminetetraacetic acid (EDTA); N-(4-Nitro-2-phenoxyphenyl)methanesulfonamide (nimesulide); thin layer chromatography (TLC); quantitative polymerase chain reaction (qRT-PCR); arachidonic acid (AA); periaqueductal gray (PAG); tris(hydroxymethyl)aminomethane (tris)

Recommended Section Assignment: Neuropharmacology

JPET Fast Forward. Published on August 11, 2010 as DOI: 10.1124/jpet.110.168831
This article has not been copyedited and formatted. The final version may differ from this version.

Abstract

Cyclooxygenase-2 (COX-2) mediates inflammation and contributes to neurodegeneration. Best known for its pathological upregulation, COX-2 is also constitutively expressed within the brain and mediates synaptic transmission through prostaglandin synthesis. Along with arachidonic acid, COX-2 oxygenates the endocannabinoids anandamide (AEA) and 2-arachidonoylglycerol *in vitro*. Inhibition of COX-2 enhances retrograde signaling in the hippocampus, suggesting COX-2 mediates endocannabinoid tone in healthy brain. The degree to which COX-2 may regulate endocannabinoid metabolism *in vivo* is currently unclear. Therefore, we explored the effect of COX-2 inhibition upon [^{3}H]AEA metabolism in mouse brain. Although AEA is primarily hydrolyzed by fatty acid amide hydrolase (FAAH), *ex vivo* autoradiography revealed that COX-2 inhibition by nimesulide redirected [^{3}H]AEA substrate from COX-2 to FAAH in the cortex, hippocampus, thalamus, and periaqueductal gray. These data indicate that COX-2 possesses the capacity to metabolize AEA *in vivo* and can compete with FAAH for AEA in several brain regions. Temporal fluctuations in COX-2 expression were observed in the brain, with an increase in COX-2 protein and mRNA in the hippocampus at midnight compared to noon. COX-2 immunolocalization was robust in the hippocampus and several cortical regions. Although most regions exhibited no temporal changes in COX-2 immunolocalization, increased numbers of immunoreactive cells were detected at midnight in layers II and III of the somatosensory and visual cortices. These temporal variations in COX-2 distribution reduced the enzyme's contribution towards [^{3}H]AEA metabolism in the somatosensory cortex at midnight. Taken together, our findings establish COX-2 as a mediator of regional AEA metabolism in mouse brain.

Introduction

Cyclooxygenase-2 (COX-2) produces prostaglandins through oxygenation of arachidonic acid. Numerous functions and pathological phenomena have been attributed to the products of COX-2 in the central nervous system. Most notably, COX-2 is upregulated in response to excitotoxicity or tissue damage. This pathological process leads to an increase in prostaglandin levels and additional neuronal damage (For review, see (Yang and Chen, 2008)).

In healthy nervous systems, COX-2 is constitutively expressed with localization primarily in the hippocampus, cortex, and amygdala (Yamagata et al., 1993). On a subcellular level, COX-2 immunoreactivity (COX-2 IR) is primarily in the perikarion and proximal dendrites (Yamagata et al., 1993). Electron microscopy studies localized rat brain COX-2 to endomembranes in dendrites near synaptic inputs from axon terminals (Wang et al., 2005).

Constitutive COX-2 activity and expression mediates long term potentiation (LTP) in mice (Chen et al., 2002) and rats (Slanina et al., 2005; Akaneya and Tsumoto, 2006) and depression (LTD) in rats (Murray and O'Connor, 2003). The promotion of LTP by COX-2 likely results from prostaglandin E2 activation of the prostaglandin E2 receptor, as nimesulide-induced reductions of LTP in the mouse dentate gyrus can be rescued by administering prostaglandin E2 (Chen et al., 2002), and receptor gene suppression reduces LTP in the visual cortex (Akaneya and Tsumoto, 2006). Overall, COX-2's localization pattern, along with its association with synaptic plasticity suggests a major role for this enzyme in the processes of learning and memory (For review, see (Yang and Chen, 2008)).

In addition to metabolizing arachidonic acid, COX-2 oxygenates endocannabinoids, producing prostamides and prostaglandin glycerol esters (Yu et al., 1997; Kozak et al., 2002). This discovery is not surprising, as endocannabinoids are structurally similar to arachidonic acid,

and the omega fatty acid portion of molecules from both groups interacts effectively with amino acids in COX-2's active site (Kozak et al., 2003)

Although the endogenous production of oxygenated endocannabinoid products by COX-2 is well documented, the functions of these recently discovered signaling molecules and their receptor targets are still being elucidated. The first study showing a signaling role for an oxygenated endocannabinoid reported that prostaglandin E2 glycerol ester, an oxidative metabolite of 2-arachidonoylglycerol (2-AG), significantly increased miniature inhibitory postsynaptic current frequency in cultured hippocampal neurons (Sang et al., 2006). In a subsequent publication, the same authors showed in hippocampal cultures that PGE2-G enhances excitatory glutamatergic synaptic transmission and promotes neurodegeneration (Sang et al., 2007). To date, it is not known what receptor(s) compounds such as PGE2-G activate. It is interesting to note, however, that these oxidative products act in direct opposition to endocannabinoids, which have long been shown to exhibit neuroprotective effects (For review, (Galve-Roperh et al., 2008).

Although COX-2 metabolizes endocannabinoids, it is widely accepted that endogenous cannabinoids are primarily hydrolyzed by fatty acid amide hydrolase (FAAH) and monoacylglycerol lipase (MGL). FAAH is widely distributed throughout the mouse brain (Egertova et al., 2003) and efficiently metabolizes the endocannabinoids anandamide (AEA) and 2-AG. Transgenic mice lacking FAAH possess elevated endogenous AEA levels, suggesting that FAAH is the principal metabolizing enzyme of AEA in the mouse (Cravatt et al., 2001; Lichtman et al., 2002). A recently published manuscript has demonstrated that activity-dependent changes in AEA tone mediate the selective "local tuning" of hippocampal inhibitory synapses(Kim and Alger, 2010). The observed changes in AEA tone were regulated by

fluctuations in local FAAH activity. Like FAAH, MGL is also widely expressed in the brain (Dinh et al., 2002) and metabolizes 2-AG but not AEA (Long et al., 2009).

While COX-2 is not considered a major endocannabinoid metabolizing enzyme, the oxygenation of endocannabinoids is physiologically important, as COX-2 inhibition potentiates rat hippocampal 2-AG signaling (Kim and Alger, 2004). Therefore, COX-2 likely regulates hippocampal endocannabinoid tone and may compete with FAAH and/or MGL for endocannabinoid substrates.

In this study, we employed a novel *ex vivo* FAAH imaging technique (Glaser et al., 2006) and the selective COX-2 inhibitor nimesulide to examine whether endogenous COX-2 activity competes with FAAH for [^{3}H]AEA metabolism in the brains of live mice. A previous report identified nimesulide as having no effects upon FAAH activity (Fowler et al., 2003). We examined eleven brain regions in order to expand upon prior work (Kim and Alger, 2004; Slanina and Schweitzer, 2005) that was restricted to hippocampal neurons possessing high endogenous expression of COX-2, FAAH and MGL. In addition, we analyzed temporal changes in COX-2 expression and localization in mouse brains by conducting experiments at the midpoint of the light and dark cycles, and studied whether temporal changes in COX-2 distribution affected regional [^{3}H]AEA metabolism.

Methods

Animals:

C57BL/6 mice (Taconic Farms, Germantown, NY) weighing approximately 25g were kept in LD 12:12. Mice were studied at the midpoint of the light and dark cycle. All mice were

maintained with free access to food and water according to the federal guidelines for the care and use of animals. These studies followed international guidelines on the ethical use of animals in research, with animal numbers and their suffering kept to a minimum. These studies were approved by the Institutional Review Committee.

Regional COX-2 western blots:

At the midpoint of the light and dark period, regional brain dissections were performed on six mice in each time point, and tissue homogenized in chilled Tris + 1mM EDTA + complete Mini EDTA acid -free protease inhibitor cocktail (Roche Diagnostics, Mannheim, Germany). Once protein concentrations were determined by BCA protein assay (Pierce Chemical, Rockford, IL), samples (40 μg of protein/lane) were run on a 10% SDS-PAGE gel. Following transfer to a nitrocellulose membrane at 100V for 25 min, blots were blocked in 5% non-fat dry milk in PBS Tween (PBST) for one hour and probed for one hour with polyclonal rabbit COX-2 antibody directed against aa 584-598 of murine COX-2 (catalog # 160126 lot # 155350 Cayman Chemical, Ann Arbor, MI) at a final concentration range of 1:100 to 1:400 or monoclonal mouse anti-β actin antibody directed against aa 1-14 of Xenopus laevis actin (AbCam, Inc. Cambridge, MA) at a final concentration of 1:20,000. The blots were rinsed three times with phosphate buffered saline tween-20 (PBST) followed by incubation with goat anti-mouse or goat anti-rabbit IgG horse radish peroxidase -conjugated antibodies (Molecular Probes, Eugene, OR) for 1 hour. Following three rinses with PBST, blots were developed using the Immun-star HRP substrate (Bio-Rad, Hercules, CA) and exposed to film. Temporal changes in regional COX-2 protein levels were determined by normalizing COX-2 levels to β-actin levels within the same lane, and

comparing samples by densitometry using Image J software. Significance was determined by unpaired 2-Tailed T-test using (GraphPad Software Inc., San Diego, CA)..

COX-2 immunolocalization:

Wild-type C57BL/6 mice were kept at LD12:12. Six hours after the onset of the light or dark period ('noon' and 'midnight', respectively), mice were deeply anesthetized and perfused with 3% formaldehyde in saline. Brains were isolated and post-fixed for another 4 hours in 3% formaldehyde, then cryoprotected in 30% sucrose. Fixed brains were embedded in 3% gelatin and 30% egg albumin and frozen in liquid nitrogen-cooled isopentane. For all immunofluorescence studies, noon and midnight cryosections (10 μm thick) were run simultaneously. Statistical analysis (Table 1) compared samples processed at the same time. Six mice were used for each time point. Sections were rinsed, then blocked for 20 min in 2% normal goat serum, then incubated overnight at 4°C in the rabbit anti-COX-2 diluted 1:150. After washing in PBS, tissue was blocked again and incubated with donkey-anti-rabbit-FITC (1:800) (Jackson Immuno Research Laboratories, West Grove, PA) for 35 min at 37°C.

Slides were rinsed then coverslipped with Vectashield (Vector Laboratories, Burlingham, CA). Sections were observed with a Zeiss epifluorescence microscope with filter sets that were optimized for FITC viewing. Controls for COX-2 IR were prepared both by omitting the primary antibody and following overnight preadsorption of the COX-2 antiserum with a 10-fold molar excess of the immunizing peptide antigen.

***In vitro* COX-2 activity time course for determining nimesulide bioavailability:**

JPET Fast Forward. Published on August 11, 2010 as DOI: 10.1124/jpet.110.168831
This article has not been copyedited and formatted. The final version may differ from this version.

Mouse brains were isolated 15, 30, and 45 min following the i.p. administration of 25 mg/kg N-(4-Nitro-2-phenoxyphenyl)methanesulfonamide (nimesulide) (Cayman Chemical) in 1:4:5 ethanol: alkamus 620 (Rhone-Poulenc, Princeton, NJ): saline and immediately homogenized on ice. Control homogenates were from mice administered vehicle only. Three mice were used in each condition. Homogenates were normalized for protein levels and assayed for tissue nimesulide levels with an *in vitro* COX-2 activity assay (a modified version of a previously published protocol(Kalgutkar et al., 1998). Human recombinant COX-2 (Cayman Chemical) (11 units per sample) was pre-incubated on ice for 30 minutes in 100 mM tris-HCl buffer + 1mM EDTA (pH 8.0) with 0.47% phenol, 1 µM hematin, 40 µM CAY10397 (a selective prostaglandin dehydrogenase inhibitor), and 225 mg of brain homogenate. Following the pre-incubation, 23.3 nCi [1-14C]arachidonic acid (Perkin Elmer, Waltham, MA) and 1µM unlabeled arachidonic acid was added to each tube (final volume = 300 µl), and samples were transferred to a 37°C shaker water bath for 10 minutes. The incubation was terminated upon the addition of chilled diethyl ether/methanol/1 M citrate (30:4:1), pH 4.0, containing butylated hydroxyanisole (an antioxidant) (10 mg) and unlabeled arachidonic acid (10 mg). Samples were centrifuged and the organic phase spotted on a thin-layer chromatography (TLC) plate (Amersham, Arlington Heights, IL). The TLC was run at 4°C in a mobile phase consisting of ethyl acetate/dichloromethane (methylene chloride)/acetic acid (75:25:1). Each sample lane was cut into 1cm squares. Each square was added to a tube containing scintillation fluid and the total radioactivity determined by scintillation counting. The inhibition of prostanoid generation by nimesulide present in the homogenates was compared between control samples and homogenates generated at various times following nimesulide administration. Significance was determined by

paired 2-Tailed T-test using Excel (Microsoft). Data were graphed using GraphPad Prism 4 (GraphPad Software Inc., San Diego, CA).

***In vitro* FAAH enzyme activity assays:**

Six hours after the onset of the light and dark period, regional brain dissections were performed on six mice for each time point. Following tissue homogenization in Tris + 1mM EDTA on ice, protein concentrations were determined by BCA protein assay (Pierce Chemical, Rockford, IL). FAAH activity assays were performed according to published methods (Deutsch and Chin, 1993)**.** Briefly, 300 µg of regional homogenate, 500 µg fatty acid-free bovine serum albumin, 100 µM AEA (Cayman Chemical, Ann Arbor, MI) plus 0.22 µCi arachidonoyl ethanolamide [ethanolamine-1-3H] (a generous gift from the National Institute on Drug Abuse, Bethesda, MD) were incubated in Tris + 1mM EDTA pH 7.6 at 37°C in triplicate for fifteen minutes while shaking. The reactions were terminated by the addition of 2 volumes of 1:1 chloroform/methanol. Samples were centrifuged, and the aqueous phase measured by liquid scintillation counting. The rates of AEA hydrolysis/mg protein/ hr were compared between noon and midnight regional homogenates. Data were graphed and significance determined by unpaired 2-Tailed T-test with a Bonferroni's correction using GraphPad Prism 4 (GraphPad Software Inc.).

***Ex vivo* autoradiography of brain FAAH activity:**

Radiolabeled AEA [arachidonoyl 5,6,8,9,11,12,14,15-3 H] was a generous gift from the NIDA Drug Inventory Supply Program. AEA (Cayman Chemical) and [^{3}H]AEA were dissolved in a 1:1:18 mixture of ethanol: alkamus-620: saline. Mice were *i.v* administered 1 mg/kg AEA +

2 mCi/kg [^{3}H]AEA. Fifteen minutes following injection, mice were sacrificed and their brains promptly transferred to a beaker containing iced saline, in order to minimize further diffusion and protein-mediated processes. Half of the cerebellum and a blood sample were homogenized, extracted in 1:1 chloroform:methanol, and analyzed by scintillation counting and thin layer chromatography (solvent system was 6:3:1 ethylacetate:hexane: acetic acid(Deutsch and Chin, 1993)), in order to quantify total tritium accumulation, and [^{3}H]AEA breakdown in these tissues. Chilled brains were transferred into iced 2% formaldehyde + 2% glutaraldehyde in phosphate buffer for one hour. The brains were then washed three times with iced phosphate buffer, and cryoprotected at 4°C in 30% sucrose in PB. Serial 15µm cryosections were generated, and images acquired for ten hours using the BetaImager (Biospace, Paris, France).

Autoradiography analysis:

Serial sections were analyzed, and surface radioactivity (cpm/mm^2) in regions of interest quantified using BetaVision+ image analysis software (Biospace Mesures, Paris, France). Data were entered into Excel (Microsoft Corp., Seattle, WA), and average regional tritium accumulation/mm^2, representing AEA and its metabolites, was determined. Six mice were used for each condition. Regional surface activities of each mouse were normalized by dividing the activity of each region over that of the pontine nuclei (the region of lowest tritium accumulation) of the same mouse. Normalization enabled regional comparison among animals with slightly different levels of brain tritium uptake. Standard error was calculated using Excel. Data were graphed, and one-way analysis of variance with Dunnett's post test was performed to determine significance between noon and midnight samples using GraphPad Prism 4 (Graph Pad Software Inc.).

JPET Fast Forward. Published on August 11, 2010 as DOI: 10.1124/jpet.110.168831
This article has not been copyedited and formatted. The final version may differ from this version.

Quantitative real time polymerase chain reaction (qRT-PCR):

At the midpoint of the light and dark period, regional dissections were performed on six mice and RNA extracted using the RNeasy mini kit (Qiagen, Valencia, CA). One microgram of RNA was subjected to cDNA synthesis using the Superscript III first strand synthesis kit (Invitrogen, Carlsbad, CA). qRT-PCR analysis was performed using the StepOne Plus Real-Time PCR system (Applied Biosystems, Foster City, CA) and the following primers: COX-2 (forward: 5'-AGGACTGGGCCATGGAGT-3' and reverse: 5'-ACCTCTCCACCAATGACCTG-3') and β-actin (forward: 5'-GACGGCCAGGTCATCACTAT-3' and reverse: 5'-CGGATGTCAACGTCACACTT-3'). Each 20 µl reaction (performed in triplicate) contained cDNA, 100 nM primer mix, and 10 µl Power SYBR Green PCR Master Mix (Applied Biosystems, Foster City, CA). The cycling conditions were as follows: 95^{o}C for 10 min, followed by 40 cycles at 95^{o}C for 15 sec and 60^{o}C for 60 sec. Negative controls lacking cDNA were included for all reactions. Amplification levels were determined using the delta delta Ct method with β-actin serving as the housekeeping gene.

Results

Temporal changes in COX-2 distribution

The regional distribution of COX-2 was compared at noon and midnight by western blot (Fig.1). A control western blot against whole brain homogenate showed one band at ~75 kDa, which was not detected in cerebellar homogenates, or in whole brain homogenates following pre-adsorption with immunizing peptide (Fig. 1A and B). Brains were harvested at the midpoint of the light and dark cycle, and regional dissections performed. The cortex, hippocampus, striatum,

and thalamus were homogenized, and analyzed by western blot. All regions were COX-2 immunoreactive, with the cortex and hippocampus exhibiting the most immunoreactivity (Fig. 1C). Increases in COX-2 protein levels were observed in midnight hippocampal samples ($p<0.05$) (Fig. 1D). Quantitative real-time PCR (qRT-PCR) corroborated the elevated expression of COX-2 in midnight hippocampi ($p<0.05$) compared to noon samples (Fig. 2). COX-2 mRNA was also detected in cortical, striatal, and thalamic samples, although their levels did not vary ($p>0.05$) with a temporal pattern.

As temporal changes in COX-2 protein and mRNA levels were detected, we performed immunohistochemistry on brains collected at noon and midnight to detect potential temporal changes in COX-2 immunoreactive cell populations. COX-2 immunoreactivity (COX-2 IR) was most robust in the hippocampus and various cortical regions, including the piriform cortex, somatosensory cortex, and visual cortex (Fig. 3). In the somatosensory and visual cortices (Fig. 3A-H), COX-2 IR was observed in laminae II, II, V, and VI. When comparing noon and midnight brain samples, changes in COX-2-IR cortical populations were observed, with a higher ($p<0.01$) ratio of immunoreactive profiles in laminae II/III relative to laminae V/VI in midnight somatosensory cortex and visual cortex samples (Table 1). Therefore, although COX-2 expression does not increase in the cortex, COX-2 distribution in the somatosensory and visual cortices change, with additional profiles exhibiting COX-2 IR at midnight.

Several other brain regions exhibited robust COX-2 IR, including the piriform cortex (Fig. 3I and J), hippocampus (Fig. 3K-P), and amygdala (Fig. 3Q and R). In the hippocampus (Fig. 3K-P), COX-2 IR was concentrated in CA2 and CA3, with little immunoreactivity observed in the dentate gyrus or CA1. Both the piriform cortex and CA2 and CA3 of the

hippocampus appeared to have increased COX-2 IR at midnight. Although COX-2 expression and protein levels were detected in the striatum and thalamus (Figs. 1 and 2), COX-2 IR was too diffuse to reliably analyze in these regions. Similarly, no COX-2 IR was detected in the periaqueductal gray (data not shown).

COX-2 competes with FAAH for [^{3}H]AEA substrate.

COX-2 is known to oxidize endogenous AEA and 2-AG (Yu et al., 1997; Kozak et al., 2002) and its inhibition potentiates cannabinoid receptor signaling in the hippocampus (Kim and Alger, 2004). Therefore, we performed the first study to estimate the contribution of COX-2 activity toward global AEA metabolism in the mouse brain employing an *ex vivo* autoradiography approach that quantifies regional [^{3}H]AEA metabolism by FAAH in intact brains (Glaser et al., 2006).

The *ex vivo* autoradiography trapping mechanism

The assay employed here quantifies local FAAH activity in intact tissue by measuring the accumulation of tritiated arachidonic acid ([^{3}H]AA) trapped in membranes following [^{3}H]AEA hydrolysis. Following the i.v. administration of [^{3}H]AEA, tracer enters the brain and is metabolized by local enzymes, including FAAH and COX-2 (Fig. 4). In the case of FAAH, [^{3}H]AEA is rapidly hydrolyzed, producing [^{3}H]AA, which is promptly incorporated into cellular membranes. If the tracer is instead oxygenated by COX-2, [^{3}H]prostamide is produced. Unlike FAAH metabolites, prostamides escape entrapment in cellular membranes and are able to freely diffuse throughout the tissue. As a result, [^{3}H]AEA metabolism by FAAH produces an increase in regional tritium levels, and metabolism by COX-2 results in no change in regional tritium

JPET Fast Forward. Published on August 11, 2010 as DOI: 10.1124/jpet.110.168831
This article has not been copyedited and formatted. The final version may differ from this version.

levels. However, if both enzymes are co-expressed, [^{3}H]AEA metabolism by COX-2 would reduce local [^{3}H]AEA availability to FAAH, thereby reducing the accumulation of tritiated FAAH metabolites in that region. As a result, if COX-2 and FAAH are competing locally for [^{3}H]AEA substrate, this autoradiography assay will detect a reduction in regional tritium accumulation.

Nimesulide administration inhibits COX-2 but not FAAH in the brain

To discern between FAAH and COX-2 activity, we imaged brains following i.p. administration of vehicle or nimesulide, a selective competitive COX-2 inhibitor. Prior to conducting brain imaging studies, we determined the degree of nimesulide penetration into the brain following i.p. administration with an *in vitro* COX-2 activity assay. We harvested brains at 15 to 45 minutes following the i.p. administration of 25 mg/kg nimesulide or vehicle. Endogenous COX-2 activity in healthy brain was too low to detect by *in vitro* enzymatic assays (data not shown). In contrast, purified COX-2 activity was readily detectable. Therefore, the presence of nimesulide in brains was determined by the brain homogenates' ability to inhibit purified COX-2 in an *in vitro* activity assay. Compared to vehicle-treated homogenates, purified COX-2 activity was significantly reduced ($p<0.05$) in nimesulide-treated homogenates that were generated at least 30 minutes following i.p. administration (Fig. 5). These data indicate that ample nimesulide had entered the brain under the assay conditions selected for the autoradiography experiments. We next conducted *in vitro* FAAH activity assays using the same nimesulide-treated and control homogenates. We detected no difference in regional activity between control and nimesulide-treated samples (Fig. 6). Collectively, these results indicate that

JPET Fast Forward. Published on August 11, 2010 as DOI: 10.1124/jpet.110.168831
This article has not been copyedited and formatted. The final version may differ from this version.

COX-2, but not FAAH, will be inhibited in autoradiography experiments performed 30 minutes following nimesulide administration.

Ex vivo autoradiography

We used autoradiography to examine the impact of COX-2 inhibition upon regional [^{3}H]AEA metabolism by FAAH at noon and midnight. Both nimesulide-treated and vehicle treated brains exhibited robust tritium accumulation, especially in the cortex and hippocampus (Fig. 7). At noon, nimesulide treatment dramatically elevated ($p<0.05$) tritium accumulation in the hippocampus, somatosensory cortex, piriform cortex, thalamus, and periaqueductal gray (PAG) without affecting the other brain regions examined (Fig. 8a). At midnight, nimesulide treatment similarly increased ($p<0.05$) tritium accumulation in the hippocampus, somatosensory cortex, thalamus, and piriform cortex. Midnight control and nimesulide-treated brains exhibited similar levels of tritium in the PAG ($p>0.05$) (Fig. 8b), suggesting reduced metabolism of [^{3}H]AEA by COX-2 at midnight relative to noon. Compared to control samples, nimesulide significantly ($p<0.05$) altered tritium accumulation in the somatosensory cortex at both noon and midnight. However, by comparing the two time points, it was discovered that nimesulide treatment exhibited significantly less effect ($p<0.05$) at midnight relative to noon.

Discussion

In the brain, COX-2 mediates synaptic transmission by synthesizing neuromodulatory prostaglandins (For review, see (Yang and Chen, 2008)). Here, we report that COX-2 is capable of metabolizing the endocannabinoid AEA *in vivo*. Our *ex-vivo* imaging method unmasked an

unexpectedly robust contribution by COX-2 toward global AEA metabolism in the mouse brain, thereby ascribing functional significance for COX-2 in endocannabinoid metabolism. .

This is the first study to describe the influence of regional COX-2 activity upon AEA hydrolysis by FAAH. Unlike traditional enzyme assays utilizing tissue homogenates, our *ex vivo* imaging method is ideally suited for the study of two enzymes competing for substrate at the regional level. We utilized nimesulide, a selective COX-2 inhibitor (see Figs. 5 and 6), to discern [^{3}H]AEA metabolism by FAAH and COX-2. As described earlier, tracer metabolism by FAAH produces [^{3}H]AA, which is promptly trapped in cellular membranes. Unlike [^{3}H]AA, COX-2 metabolites are expected to escape such trapping mechanisms and freely diffuse throughout the brain. Therefore, regions with significant COX-2 [^{3}H]AEA metabolism will, upon nimesulide administration, instead shunt [^{3}H]AEA towards FAAH, resulting in increased [^{3}H]AA being trapped in regional membranes. Following nimesulide administration, we observed increased tritium accumulation at both noon and midnight in the hippocampus, thalamus, piriform cortex, and somatosensory cortex (Fig. 8). Nimesulide administration also caused an increase in noon PAG tritium accumulation. These data suggest that competition between FAAH and COX-2 for AEA may serve as a point of regulation for brain AEA signaling in numerous regions.

Competition for substrate necessitates close proximity between enzymes within the same brain region. As expected, the COX-2 IR pattern in C57BL/6 mice is similar to both the distribution of COX-2 in rat brains (Yamagata et al., 1993; Wang et al., 2005), and the distribution of FAAH in C57BL/6 mice (Egertova et al., 2003). Both COX-2 (Fig. 3) and FAAH immunoreactivity (FAAH IR) (Egertova et al., 2003) are found throughout the cortex, with prominent immunoreactivity in the piriform cortex and layers II and III of the somatosensory and visual cortices. In the hippocampus, both COX-2 and FAAH IR exhibit robust

immunoreactivity, although COX-2 IR is primarily concentrated in CA2 and CA3. FAAH IR was also prominent in most thalamic nuclei. Although COX-2 IR was not detected in this region (Fig. 3), both COX-2 protein (Fig. 1) and mRNA (Fig. 2) were detected, suggesting low levels of the enzyme exist in the thalamus. It is noteworthy that regions consistently exhibiting nimesulide-dependent increases in tritium accumulation (Fig. 8) express both COX-2 and FAAH (Egertova et al., 2003). These data suggest that FAAH and COX-2 are sufficiently co-localized to compete for [^{3}H]AEA substrate in these brain regions.

The autoradiography assay used in this manuscript more closely mimics endogenous AEA metabolism than *in vitro* enzyme assays providing an excess of substrate. Through autoradiography analysis, regions with robust COX-2 expression, such as the hippocampus, exhibit no more dramatic differences between control and COX-2-inhibited states than the thalamus. Similar to *in vivo* settings where endogenous AEA levels are produced in limited quantities, these results are likely due to limited substrate/tracer availability restricting COX-2 activity in control animals. These results suggest that COX-2 is expressed in several brain regions at levels in excess of what is required to metabolize endogenous substrates such as AEA, possibly to ensure the prompt metabolism of these lipid signaling molecules and prevent their accumulation near receptors.

To date, all physiology studies that show COX-2's influence over endogenous cannabinoid signaling have studied the hippocampus (Kim and Alger, 2004; Slanina and Schweitzer, 2005), the brain region exhibiting the most robust COX-2 expression. Our data reveal that even regions with modest COX-2 expression can exhibit competition between COX-2 and FAAH for [^{3}H]AEA substrate. For example, although thalamic COX-2 protein levels are too low to detect by immunofluorescence (Fig. 3), its enzymatic inhibition is sufficient to potentiate

[^{3}H]AEA hydrolysis by FAAH. These striking results suggest that COX-2's influence upon endocannabionid / endovanilloid signaling could be much more extensive than previously believed, and suggests that more physiology studies of these systems should be conducted to better ascertain COX-2's influence upon these endogenously produced signaling molecules.

Prostamides and prostaglandin glycerol esters have distinct signaling properties from both endocannabinoids and prostaglandins and do not interact with cannabinoid or prostaglandin receptors (For review, see Woodward et al., 2008). As expected these compounds have distinct pharmacological properties, with prostamides regulating intraocular pressure (Woodward et al., 2008) and stimulating cat iris contraction (Matias et al., 2004), and glyceryl prostaglandins mediating calcium mobilization, inositol 1,4,5-trisphosphate synthesis, and activation of protein kinase C in RAW264.7 macrophage cells (Nirodi et al., 2004). The data presented in this study suggest that nimesulide can be used to inhibit prostamide production. Not only does this increase substrate availability to FAAH, it also likely could inhibit several prostamide-mediated processes in the body.

We observed temporal changes in COX-2 expression in healthy mouse brains. Relative to noon, western blot (Fig. 1) and qRT-PCR (Fig. 2) analyses revealed an increase in COX-2 expression in hippocampal samples at midnight. Although the levels of COX-2 protein and mRNA did not vary, immunohistochemistry studies (Fig. 3) detected shifts in immunoreactive cell populations in the somatosensory and visual cortices between noon and midnight, with more immunoreactive cells in lamina II and III of midnight samples.

The temporal changes in COX-2 IR observed in the current study were generally too slight to alter the regional distribution pattern of [^{3}H]AEA metabolites between noon and midnight samples (Fig. 8). Only the somatosensory cortex exhibited a significant change

between the two time points, with the midnight nimesulide condition exhibiting significantly less effect relative to midnight control samples than noon nimesulide samples. At first glance, the autoradiography data would appear to contradict the immunoreactivity data (Fig. 3) that exhibits an increase in the number of COX-2 IR cells at midnight. However, the pattern of COX-2 IR cells changes in the somatosensory cortex between noon and midnight, and this change in distribution may result in COX-2 becoming more remote from FAAH near specific synaptic connections at midnight, thereby lessening the competition between the two enzymes for substrate.

Similar to COX-2, FAAH exhibits temporal changes in brain expression and activity. In a prior publication (Glaser and Kaczocha, 2009), we observed that FAAH activity in the mouse cerebellum and PAG fluctuated temporally, with reductions in regional activity observed in the middle of the dark cycle of the mice. Temporal changes in regional FAAH activity were monitored during this study, and were carefully discerned from any nimesulide-induced changes in regional [^{3}H]AEA metabolism. It should be noted that significant reductions in FAAH activity can alter the sensitivity of the autoradiography assay in some brain regions. For example, although PAG tritium accumulation was significantly potentiated by nimesulide at noon, nimesulide exhibited no effect in midnight PAG (Fig. 8). This is likely due to reduced midnight PAG FAAH activity (Glaser and Kaczocha, 2009) diminishing the sensitivity of the imaging assay in the PAG at midnight.

When results from the current study are grouped with prior reports demonstrating potentiation of 2-AG signaling in the hippocampus following COX-2 inhibition (Kim and Alger, 2004; Slanina and Schweitzer, 2005), the potential regulatory role of COX-2 in endocannabinoid signaling becomes even more apparent. We predict that systemic nimesulide administration

potentiates endogenous AEA signaling in mouse hippocampus, thalamus, somatosensory cortex, piriform cortex, and PAG. It is conceivable that COX-2 also mediates the signaling of other lipid molecules that share similar metabolic pathways to AEA and 2-AG.

In conclusion, this study reveals competition between FAAH and COX-2 for common substrates in multiple brain regions of the mouse. As a result, activity of one enzyme may reduce substrate availability to the other. Just as inhibiting rat hippocampal COX-2 potentiates endocannabinoid signaling (Kim and Alger, 2004; Slanina and Schweitzer, 2005), it is equally likely that FAAH inhibition might potentiate endogenous prostamide signaling within the brain.

References

Akaneya Y and Tsumoto T (2006) Bidirectional trafficking of prostaglandin E2 receptors involved in long-term potentiation in visual cortex. *J Neurosci* **26**:10209-10221.

Chen C, Magee JC and Bazan NG (2002) Cyclooxygenase-2 regulates prostaglandin E2 signaling in hippocampal long-term synaptic plasticity. *J Neurophysiol* **87**:2851-2857.

Cravatt BF, Demarest K, Patricelli MP, Bracey MH, Giang DK, Martin BR and Lichtman AH (2001) Supersensitivity to anandamide and enhanced endogenous cannabinoid signaling in mice lacking fatty acid amide hydrolase. *Proc Natl Acad Sci U S A* **98**:9371-9376.

Deutsch DG and Chin SA (1993) Enzymatic synthesis and degradation of anandamide, a cannabinoid receptor agonist. *Biochem Pharmacol* **46**:791-796.

Dinh TP, Freund TF and Piomelli D (2002) A role for monoglyceride lipase in 2-arachidonoylglycerol inactivation. *Chem Phys Lipids* **121**:149-158.

Egertova M, Cravatt BF and Elphick MR (2003) Comparative analysis of fatty acid amide hydrolase and cb(1) cannabinoid receptor expression in the mouse brain: evidence of a widespread role for fatty acid amide hydrolase in regulation of endocannabinoid signaling. *Neuroscience* **119**:481-496.

Fowler CJ, Holt S and Tiger G (2003) Acidic nonsteroidal anti-inflammatory drugs inhibit rat brain fatty acid amide hydrolase in a pH-dependent manner. *J Enzyme Inhib Med Chem* **18**:55-58.

Galve-Roperh I, Aguado T, Palazuelos J and Guzman M (2008) Mechanisms of control of neuron survival by the endocannabinoid system. *Curr Pharm Des* **14**:2279-2288.

Glaser ST, Gatley SJ and Gifford AN (2006) Ex vivo imaging of fatty acid amide hydrolase activity and its inhibition in the mouse brain. *J Pharmacol Exp Ther* **316**:1088-1097.

Glaser ST and Kaczocha M (2009) Temporal changes in mouse brain fatty acid amide hydrolase activity. *Neuroscience* **163**:594-600.

Kalgutkar AS, Crews BC, Rowlinson SW, Garner C, Seibert K and Marnett LJ (1998) Aspirin-like molecules that covalently inactivate cyclooxygenase-2. *Science* **280**:1268-1270.

Kim J and Alger BE (2004) Inhibition of cyclooxygenase-2 potentiates retrograde endocannabinoid effects in hippocampus. *Nat Neurosci* **7**:697-698.

Kim J and Alger BE (2010) Reduction in endocannabinoid tone is a homeostatic mechanism for specific inhibitory synapses. *Nat Neurosci*.

Kozak KR, Gupta RA, Moody JS, Ji C, Boeglin WE, DuBois RN, Brash AR and Marnett LJ (2002) 15-Lipoxygenase metabolism of 2-arachidonylglycerol. Generation of a peroxisome proliferator-activated receptor alpha agonist. *J Biol Chem* **277**:23278-23286.

Kozak KR, Prusakiewicz JJ, Rowlinson SW, Prudhomme DR and Marnett LJ (2003) Amino acid determinants in cyclooxygenase-2 oxygenation of the endocannabinoid anandamide. *Biochemistry* **42**:9041-9049.

Lichtman AH, Hawkins EG, Griffin G and Cravatt BF (2002) Pharmacological activity of fatty acid amides is regulated, but not mediated, by fatty acid amide hydrolase in vivo. *J Pharmacol Exp Ther* **302**:73-79.

Long JZ, Nomura DK and Cravatt BF (2009) Characterization of monoacylglycerol lipase inhibition reveals differences in central and peripheral endocannabinoid metabolism. *Chem Biol* **16**:744-753.

Matias I, Chen J, De Petrocellis L, Bisogno T, Ligresti A, Fezza F, Krauss AH, Shi L, Protzman CE, Li C, Liang Y, Nieves AL, Kedzie KM, Burk RM, Di Marzo V and Woodward DF (2004) Prostaglandin ethanolamides (prostamides): in vitro pharmacology and metabolism. *J Pharmacol Exp Ther* **309**:745-757.

Murray HJ and O'Connor JJ (2003) A role for COX-2 and p38 mitogen activated protein kinase in long-term depression in the rat dentate gyrus in vitro. *Neuropharmacology* **44**:374-380.

Nirodi CS, Crews BC, Kozak KR, Morrow JD and Marnett LJ (2004) The glyceryl ester of prostaglandin E2 mobilizes calcium and activates signal transduction in RAW264.7 cells. *Proc Natl Acad Sci U S A* **101**:1840-1845.

Paxinos G FK (2001) *The mouse brain in stereotaxic coordinates*. Academic Press, San Diego, CA.

Sang N, Zhang J and Chen C (2006) PGE2 glycerol ester, a COX-2 oxidative metabolite of 2-arachidonoyl glycerol, modulates inhibitory synaptic transmission in mouse hippocampal neurons. *J Physiol* **572**:735-745.

Sang N, Zhang J and Chen C (2007) COX-2 oxidative metabolite of endocannabinoid 2-AG enhances excitatory glutamatergic synaptic transmission and induces neurotoxicity. *J Neurochem* **102**:1966-1977.

Slanina KA, Roberto M and Schweitzer P (2005) Endocannabinoids restrict hippocampal long-term potentiation via CB1. *Neuropharmacology* **49**:660-668.

Slanina KA and Schweitzer P (2005) Inhibition of cyclooxygenase-2 elicits a CB1-mediated decrease of excitatory transmission in rat CA1 hippocampus. *Neuropharmacology* **49**:653-659.

Wang H, Hitron IM, Iadecola C and Pickel VM (2005) Synaptic and vascular associations of neurons containing cyclooxygenase-2 and nitric oxide synthase in rat somatosensory cortex. *Cereb Cortex* **15**:1250-1260.

Woodward DF, Carling RW, Cornell CL, Fliri HG, Martos JL, Pettit SN, Liang Y and Wang JW (2008) The pharmacology and therapeutic relevance of endocannabinoid derived cyclo-oxygenase (COX)-2 products. *Pharmacol Ther* **120**:71-80.

Yamagata K, Andreasson KI, Kaufmann WE, Barnes CA and Worley PF (1993) Expression of a mitogen-inducible cyclooxygenase in brain neurons: regulation by synaptic activity and glucocorticoids. *Neuron* **11**:371-386.

Yang H and Chen C (2008) Cyclooxygenase-2 in synaptic signaling. *Curr Pharm Des* **14**:1443-1451.

Yu M, Ives D and Ramesha CS (1997) Synthesis of prostaglandin E2 ethanolamide from anandamide by cyclooxygenase-2. *J Biol Chem* **272**:21181-21186.

Footnotes:

We thank Manaf Assifin for his help developing the *in vitro* COX-2 activity assay, and Prof. Dale Deutsch for use of his laboratory equipment. This work was supported by the National Institutes of Health National Institute on Drug Abuse [1 K01 DA021806-01] (S.T.G.).

JPET Fast Forward. Published on August 11, 2010 as DOI: 10.1124/jpet.110.168831
This article has not been copyedited and formatted. The final version may differ from this version.

Legends for Figures:

Fig. 1 ***Regional COX-2 Western blots.*** Homogenates were generated from brains from six mice isolated at the midpoint of the light ("noon") and dark ("midnight") cycles, and probed for COX-2 immunoreactivity. A) Whole brain homogenate produces a single 75 kDa band that is blocked when the membrane is preincubated with immunizing peptide. B) Cerebellar homogenates lack COX-2 immunoreactivity. C) Regional expression levels of COX-2 with β-actin serving as the endogenous control. D) Regional COX-2 levels were quantified by densitometry of western blots and midnight and noon conditions compared. Expression levels were normalized to β-actin and subsequently analyzed. The data presented in the graph above represents regional normalized midnight densitometry / normalized noon densitometry. Bars represent the regional mean ±SE. Significance was determined by an unpaired two-tailed *t*-test. An increase in COX-2 protein levels was observed in hippocampal homogenates. *, $p<0.05$.

Fig. 2 ***qRT-PCR analysis of COX-2 expression in brains at noon and midnight***. Six mouse brains were dissected and the cortex, hippocampus, striatum, and thalamus subjected to RNA extraction, cDNA synthesis, and qRT-PCR analysis. Relative mRNA levels were determined with β-actin serving as the housekeeping gene. The mRNA expression levels of each region were normalized to the respective noon samples. Values represent means of at least five independent experiments performed in triplicate. *, $p < 0.05$.

Fig. 3 ***Distribution of COX-2 IR in the mouse brain at noon and midnight.*** Mice were perfused, and six brains isolated at the midpoint of their light (noon) and dark (midnight) cycles. Brains were sectioned and processed for immunofluorescence studies using a primary polyclonal

JPET Fast Forward. Published on August 11, 2010 as DOI: 10.1124/jpet.110.168831
This article has not been copyedited and formatted. The final version may differ from this version.

antibody directed against mouse COX-2. COX-2 IR was prominent throughout the cortex (1-4) and hippocampus (6-8), with additional immunoreactivity observed in the amygdala (9). In the cortex, layers II/III of the somatosensory (1N) and visual (3N) cortices exhibited robust COX-2 IR likely in pyramidal cells at noon, as layers V/VI of the somatosensory (2N) and visual (4N) cortices displayed very modest COX-2 IR. Relative to noon samples, COX-2 IR increased in layers II/III of the somatosensory (1M) and visual (3M) cortices at midnight, and remained similar to the noon samples in layers V/VI of the somatosensory (2M) and visual (4M) cortices. The piriform cortex (5N-5M) had extensive COX-2 IR at both time points, with a slight increase in the intensity of immunoreactivity in midnight samples (5M). In the hippocampus, COX-2 IR was very low in CA1 (6N -6M) and the dentate gyrus (7N-7M) at both time points, with CA2 and CA3 (8N-8M) exhibiting the majority of COX-2 IR soma in that region. CA2 and CA3 also exhibited a possible increase in fluorescence at midnight (8M) relative to noon (8N), suggesting a potential increase in hippocampal COX-2 at that time point. The amygdala (9N-9M) contained a modest number of COX-2 IR soma that did not appear to substantially change between noon and midnight. Scale bar in A = 50 μm.

Fig. 4 ***Trapping mechanism for [^{3}H]AEA metabolites.*** Following [^{3}H]AEA administration, [^{3}H]AEA enters the brain and undergoes either hydrolysis by FAAH or oxygenation by COX-2. Upon hydrolysis by FAAH, [^{3}H]AEA is converted into [^{3}H]AA, which is promptly incorporated into cellular membranes. This membranous tritium is easily imaged by *ex vivo* autoradiography and quantified. Upon oxygenation by COX-2, the [^{3}H]prostamide freely diffuses throughout the tissue.

JPET Fast Forward. Published on August 11, 2010 as DOI: 10.1124/jpet.110.168831
This article has not been copyedited and formatted. The final version may differ from this version.

Fig. 5 ***Nimesulide accumulates in the brain following i.p. administration.*** Mice were i.p. administered vehicle or 25mg/kg nimesulide and their brains were isolated 0, 15, 30, and 45 minutes later. Three mice were included at each time point. To detect the presence of nimesulide in brain, purified COX-2 enzyme was added to brain homogenates of vehicle- or nimesulide-injected mice, and the samples were tested for their ability to oxygenate [^{14}C]AA. Relative to control samples, homogenates generated 30 and 45 minutes following nimesulide administration exhibited significantly ($p<0.05$) less [^{14}C]prostaglandin generation, indicating that a substantial quantity of nimesulide accumulated in brain by these time points.

Fig. 6 ***Regional FAAH activity is not affected by nimesulide administration.*** WT mice were i.p. administered vehicle or 25 mg/kg nimesulide, and their brains isolated 0, 15, 30, and 45 minutes later. Homogenates were generated and FAAH activity determined. [^{3}H]AEA hydrolysis in control and nimesulide-treated homogenates was similar ($p>0.05$), indicating that nimesulide treatment does not alter regional FAAH activity in the brain.

Fig. 7 ***Regional tritium distribution in control and nimesulide-treated mice.*** Following the administration of 25 mg/kg nimesulide or vehicle, mice were administered 1 mg/kg + 50µCi [^{3}H]AEA and their brains processed for *ex vivo* autoradiography. Column 1 is a schematic of the regions pictured in the autoradiographs in columns 2 and 3. Analyzed regions are depicted in gray and include the (1) caudate putamen, (2) the piriform cortex, (3) the somatosensory cortex, (4) the hypothalamus, (5) the amygdala, (6) the thalamus, (7) the hippocampus, (8) the entorhinal cortex, (9) the visual cortex, (10) the periaqueductal gray (PAG), and the cerebellum. [^{3}H]AEA and its metabolites accumulated in a heterogeneous pattern in both control (column 2) and

nimesulide-treated brains (column 3), with the most accumulation observed in the cortical and thalamic regions. The images that are modified in column 1 were originally published in *The Mouse Brain in Stereotaxic Coordinates, 2nd* edition, Paxinos, plates 32, 44, and 54. Copyright Academic Press (2001).

Fig. 8 *Ex vivo* autoradiography analysis of nimesulide-induced changes in [^{3}H]AEA metabolism by FAAH. Mice were i.p. administered 25 mg/kg nimesulide or vehicle and 30 minutes later, i.v. administered 1 mg/kg AEA+50 μCi [^{3}H]AEA at the midpoint of the light ("noon") or dark ("midnight") cycle. Thirty minutes following tracer administration, brains were isolated, fixed, and processed for imaging in the BetaImager. Six mice were utilized for each time point. Regional tritium accumulation (cpm/mm^2) due to FAAH activity was quantified using BetaVision+ software. Regional tritium accumulation was normalized against tritium levels in the lateral entorhinal cortex, a brain region where nimesulide did not alter tritium accumulation and a region with no detectable COX-2 IR. Normalized regional tritium levels were compared between nimesulide-treated and control samples and significance was determined by a one-way analysis of variance with Dunnett's post test. Bars represent the regional mean ± S.E. The dotted line represents the relative value of the lateral entorhinal cortex. **A)** Noon nimesulide-induced changes in regional tritium accumulation. At noon, regional tritium accumulation, representing the accumulation of tritiated FAAH metabolites, was elevated in the PAG, hippocampus, thalamus, somatosensory cortex, and piriform cortex of nimesulide-treated mice relative to control animals (*, $p<0.05$). **B)** Midnight nimesulide-induced changes in regional tritium accumulation. Similar to noon, regional tritium accumulation at midnight was

higher in the hippocampus, thalamus, somatosensory cortex, and piriform cortex of nimesulide-treated mice relative to control animals (*, $p<0.05$).

JPET Fast Forward. Published on August 11, 2010 as DOI: 10.1124/jpet.110.168831
This article has not been copyedited and formatted. The final version may differ from this version.

Table 1 Quantification of COX-2 IR profiles in cortical laminae.

Time of day	Ave # COX-2 IR profiles Lamina II/III	Ave # COX-2 IR profiles Lamina V/VI	Ratio Lamina II/III / Lamina V/VI
noon	39.8 ± 1.8	37.7 ± 5.9	1.20 ± 0.12
midnight	57.2 ± 3.9	26.9 ± 2.4	2.20 ± 0.14**

**p<0.01

Table 1 ***Quantification of COX-2 IR profiles in cortical laminae of the somatosensory and visual cortices.*** COX-2 IR soma in cortical laminae II/ III and V/ IV were tallied in representative visual fields of 0.0339 mm^2 in mouse brains isolated at both noon and midnight. In a double-blind analysis, the ratio of immunoreactive profiles in each group of laminae was calculated for each visual field, and the average ratios and standard error calculated for noon and midnight conditions. Three visual fields from each mouse were analyzed, and six mice were examined. Significance was determined by ANOVA. Relative to noon, there was a higher average number of immunoreactive profiles in laminae II and III at midnight, and fewer COX-2 IR profiles in laminae V and VI. This caused the ratio of immunoreactive profiles in laminae II and III / laminae V and VI to significantly (**p<0.01) shift in a positive direction from noon to midnight, indicating a shift in the population of immunoreactive profiles in these cortical regions.

Fig. 1

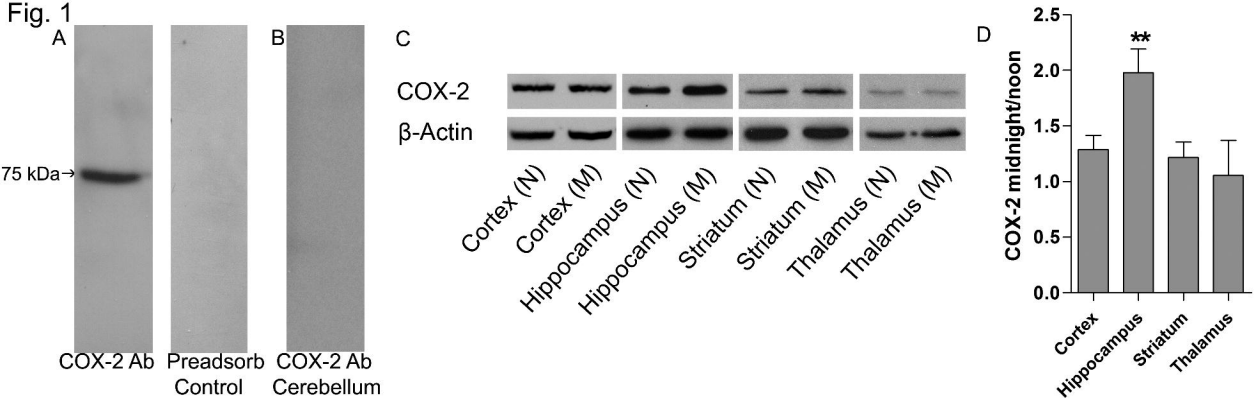
A
75 kDa→
COX-2 Ab
Preadsorb Control
B
COX-2 Ab Cerebellum
C
COX-2
β-Actin
Cortex (N)
Cortex (M)
Hippocampus (N)
Hippocampus (M)
Striatum (N)
Striatum (M)
Thalamus (N)
Thalamus (M)
D
COX-2 midnight/noon
2.5
2.0
1.5
1.0
0.5
0.0
**
Cortex
Hippocampus
Striatum
Thalamus

Fig. 2

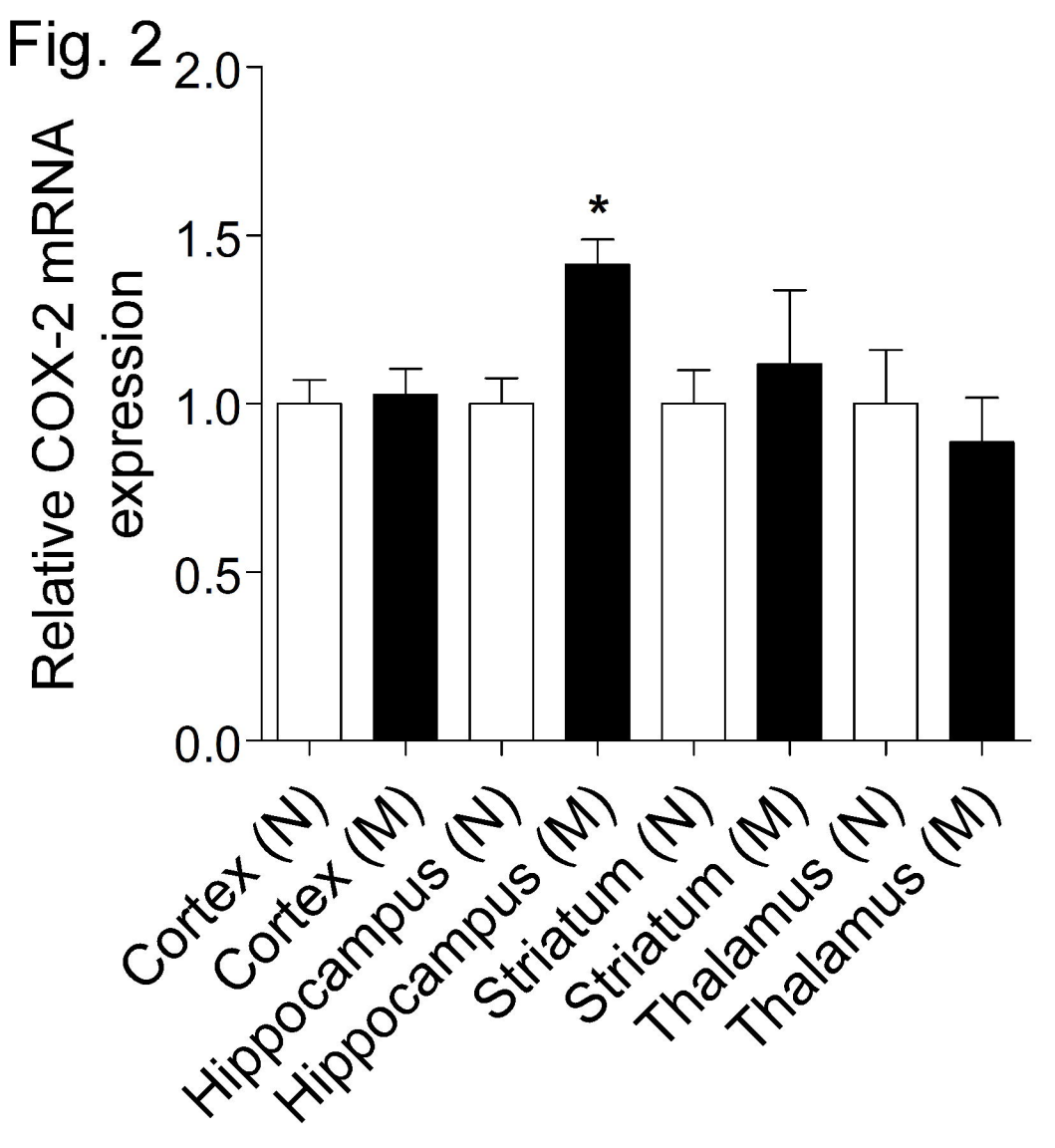
Relative COX-2 mRNA expression
2.0
1.5
1.0
0.5
0.0
*
Cortex (N)
Cortex (M)
Hippocampus (N)
Hippocampus (M)
Striatum (N)
Striatum (M)
Thalamus (N)
Thalamus (M)

Fig. 3

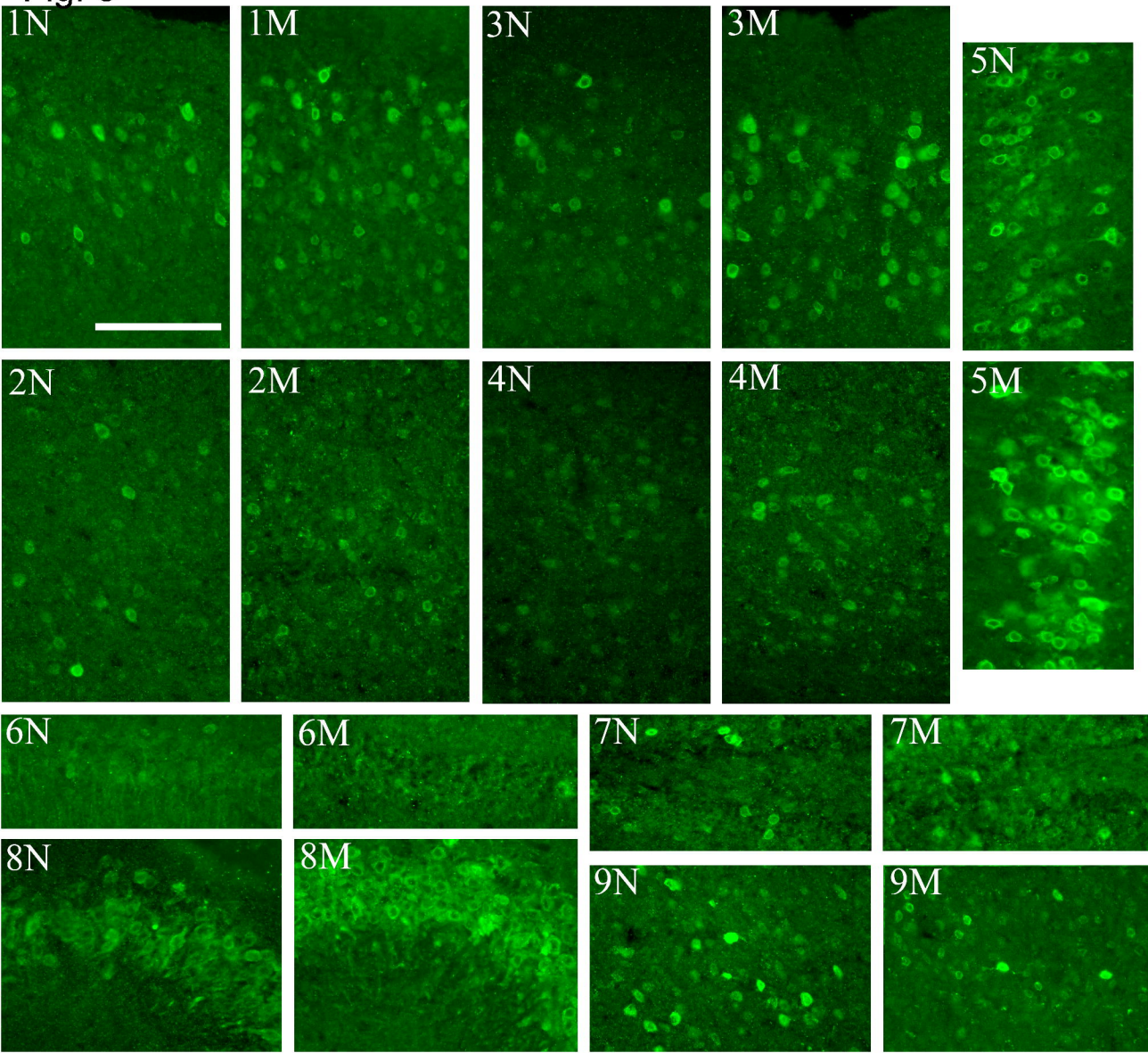

Fig. 4

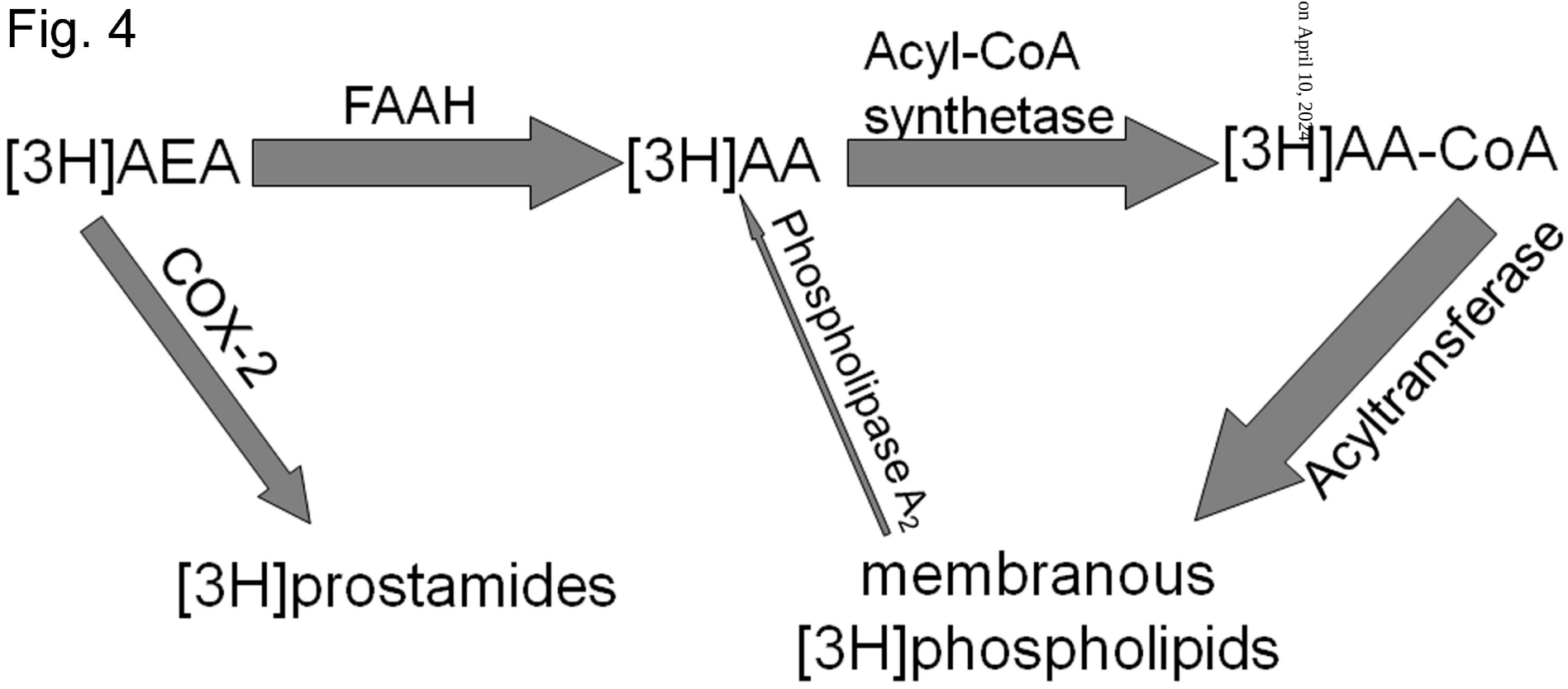

Fig. 5

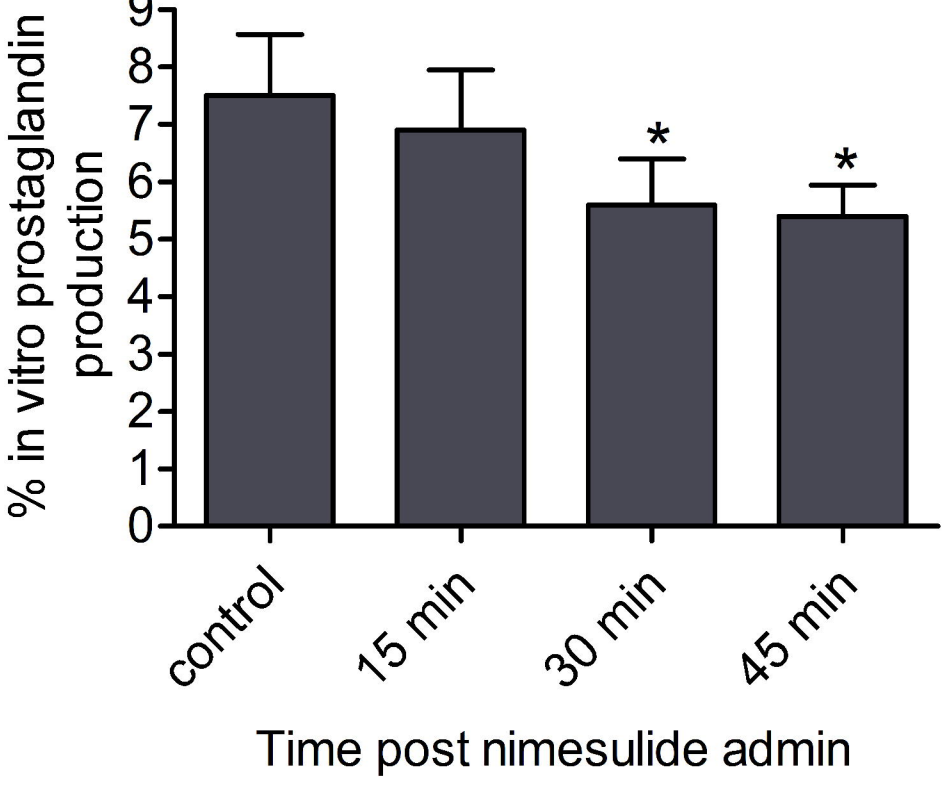
% in vitro prostaglandin production
0
1
2
3
4
5
6
7
8
9
*
*
control
15 min
30 min
45 min
Time post nimesulide admin

Fig. 6

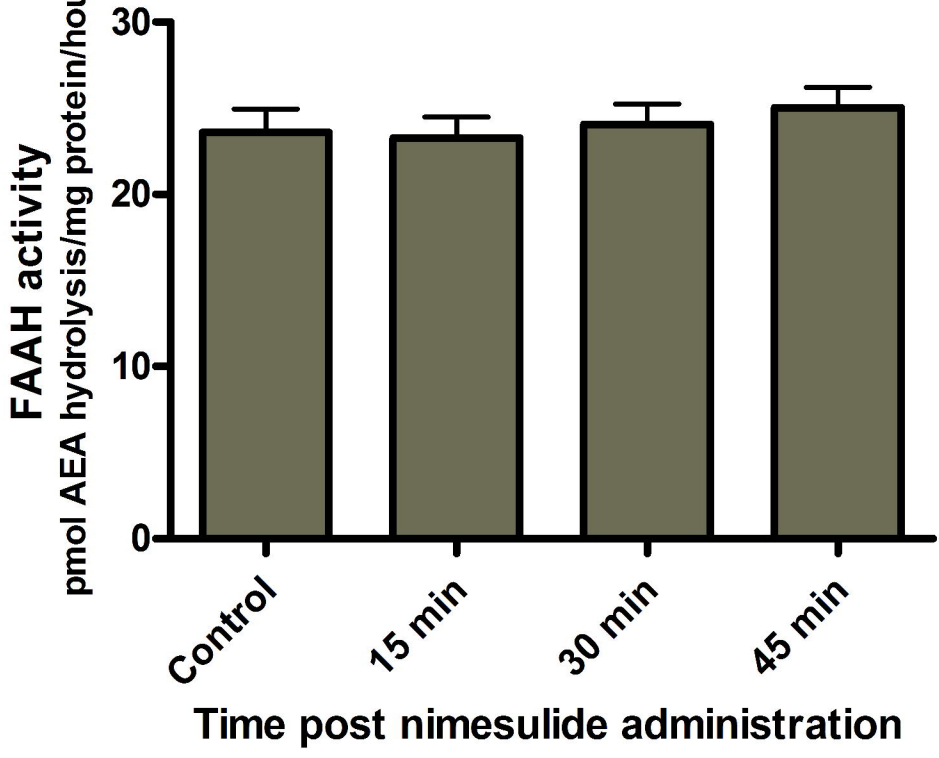
FAAH activity
pmol AEA hydrolysis/mg protein/hour
30
20
10
0
Control
15 min
30 min
45 min
Time post nimesulide administration

Fig. 7

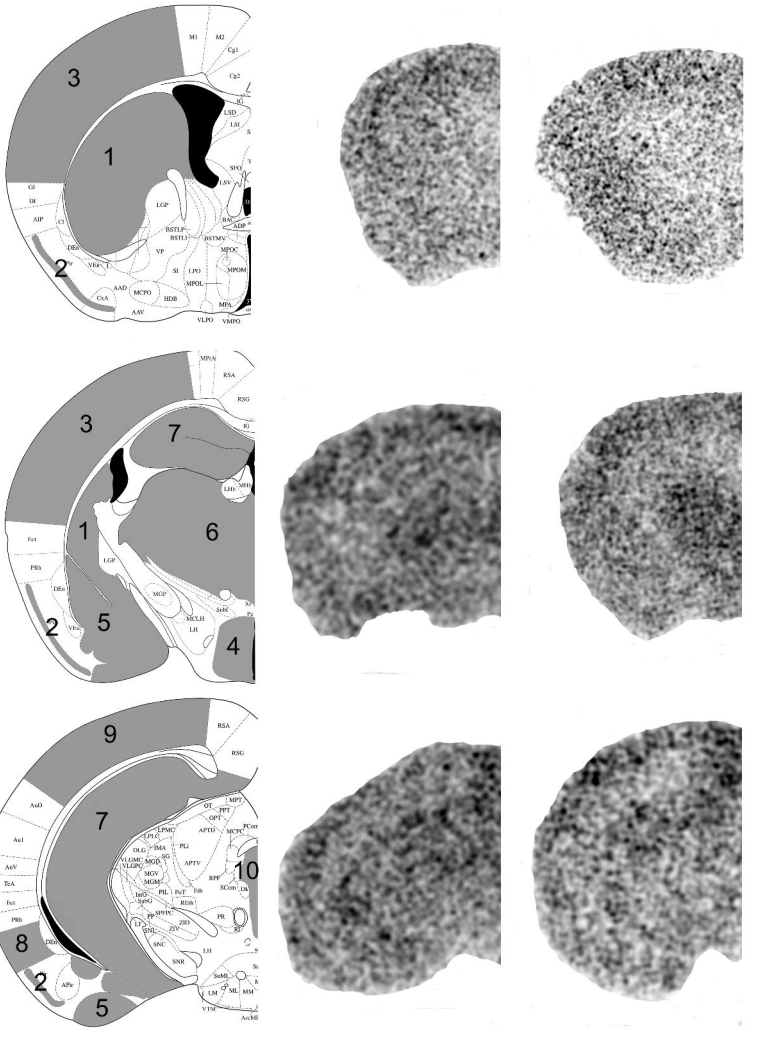
Regions
Control
Nimesulide
3
1
2
M1
M2
Cg1
Cg2
LSD
LSI
S
LSV
SFO
LGP
BAC
ADP
BSTLP
BSTLV
BSTMV
VP
MPOC
SI
LPO
MPOM
MPOL
AAD
MCPO
CxA
HDB
AAV
MPA
VLPO
VMPO
GI
DI
AIP
DEn
VEn
3
7
1
6
2
5
4
MPtA
RSA
RSG
LHb
MHb
Ect
PRh
LGP
MGP
SubI
MCLH
LH
VEn
9
7
10
8
2
5
AuD
Au1
AuV
TeA
Ect
PRh
DEn
APir
LPMC
LPLC
DLG
IMA
SG
VLGMC
VLGPC
MGD
MGV
MGM
PIL
PoT
SubG
InG
ZID
ZIV
SNC
SNR
PPT
OT
APTD
MCPC
PLL
APTV
RPF
SCom
Eth
RTdb
PR
RC
LH
SubM
LM
ML
MM
VTM
AscMl

Fig. 8

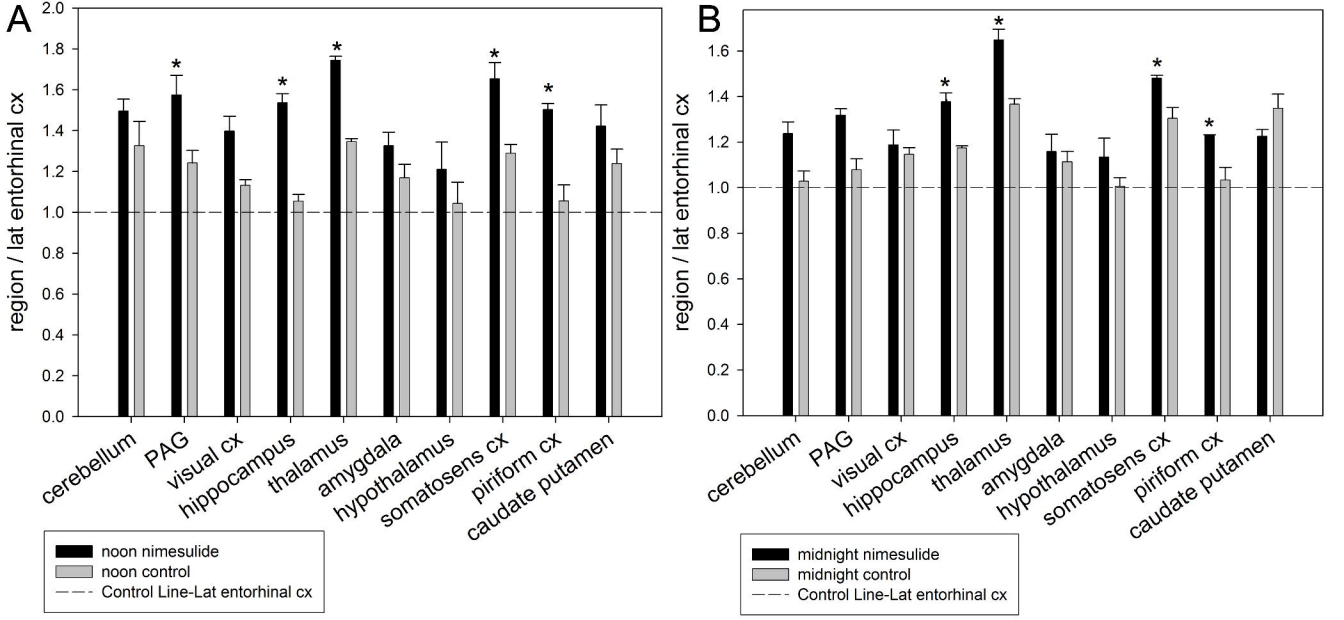
A
region / lat entorhinal cx
2.0
1.8
1.6
1.4
1.2
1.0
0.8
0.6
0.4
0.2
0.0
cerebellum
PAG
visual cx
hippocampus
thalamus
amygdala
hypothalamus
somatosens cx
piriform cx
caudate putamen
noon nimesulide
noon control
Control Line-Lat entorhinal cx
B
region / lat entorhinal cx
1.6
1.4
1.2
1.0
0.8
0.6
0.4
0.2
0.0
cerebellum
PAG
visual cx
hippocampus
thalamus
amygdala
hypothalamus
somatosens cx
piriform cx
caudate putamen
midnight nimesulide
midnight control
Control Line-Lat entorhinal cx